Nano Energy (2014) 10, 28–36

Available online at www.sciencedirect.com

ScienceDirect

journal homepage: www.elsevier.com/locate/nanoenergy

RAPID COMMUNICATION

Toward high efficiency and panel size $30 \times 40\ cm^2$ $Cu(In,Ga)Se_2$ solar cell: Investigation of modified stacking sequences of metallic precursors and pre-annealing process without Se vapor at low temperature

Tsung-Ta Wu[a,b], Jyun-Hong Huang[b,c], Fan Hu[a,b], Chia-ho Chang[b], Wen-Long Liu[a], Tsang-Hsiu Wang[a], Chang-Hong Shen[b,*], Jia-Min Shieh[b,*], Yu-Lun Chueh[a,*]

[a]*Department of Materials Science and Engineering, National Tsing-Hua University, Hsinchu 30013, Taiwan*
[b]*National Nano Device Laboratories, No.26, Prosperity Road 1, Hsinchu 30078, Taiwan*
[c]*College of photonic and Institute of Imaging and Biomedical Photonics, National Chiao Tung University, Taiwan*

Received 22 June 2014; accepted 22 July 2014
Available online 11 August 2014

KEYWORDS
$Cu(InGa)Se_2$;
Stacked precursor;
Pre-annealing;
Selenization;
Ga depth profile

Abstract
Modified stacking sequence of precursors and pre-annealing process on Se vapor at low temperature were applied to $Cu(In,Ga)Se_2$ (CIGS) solar. The remarkable improvement of efficiency (5.53–10.10% and further 11.04%) and open circuit voltage (0.41 V–0.53 V and further 0.56 V) comes from a compact, smooth microstructure, and modified depth profile of Ga with suitable thickness of CuGa multi-stacking layers in the top of precursors as well as surface bandgap enhancement *via* pre-annealing process without Se vapor followed by a specific non-toxic hydrogen-assisted solid Se vapor selenization process. The effects of microstructural, compositional and electrical characteristics of Ga distribution including accumulation and interdiffusion were examined in detail. Finally, a large-area ($40 \times 30\ cm^2$) CIGS solar cell efficiency with improved open circuit voltage (V_{OC}) and fill factor (FF) of 36% and 14% has been demonstrated, yielding a promising efficiency of ~11.04%.

*Corresponding authors.
E-mail addresses: chshen@narlabs.org.tw (C.-H. Shen), jmshieh@narlabs.org.tw (J.-M. Shieh), ylchueh@mx.nthu.edu.tw (Y.-L. Chueh).

http://dx.doi.org/10.1016/j.nanoen.2014.07.018
2211-2855/

Introduction

Compared to other thin film solar cell devices, Cu(In,Ga)Se_2 (CIGS) and related materials have been considered as the most promise candidates due to their high absorption coefficients and excellent outdoor stability, yielding the highest energy conversion efficiency and low cost [1,2]. A previous work has reported that the highest efficiency of ~20.8% for a CIGS single cell was fabricated by a co-evaporation process [3]. Advantages of controllably stoichiometric composition, smooth surface, high absorption efficiency, and better carrier collection by the co-evaporation process provide the CIGS absorber with excellent quality [4]. However, mass production by this approach for a large scale CIGS film is limited due to poor uniformity and low throughput. Sputtering process *via* Cu/In/Ga metallic precursors followed by a selenization process is a likely method to massively produce a large area solar panel. However, the low melting-point (~140 °C) pure In phases of the metallic precursors typically result in degradation of filling factor of CIGS solar cells owing to rough morphology on the CIGS layer [5-8]. The difference in thermodynamics [9] and diffusivity [10] between In and Ga leads to internal diffusion, namely accumulation of Ga, near to Mo back electrode, which results in lowing conversion efficiency due to an decrease in open circuit voltage

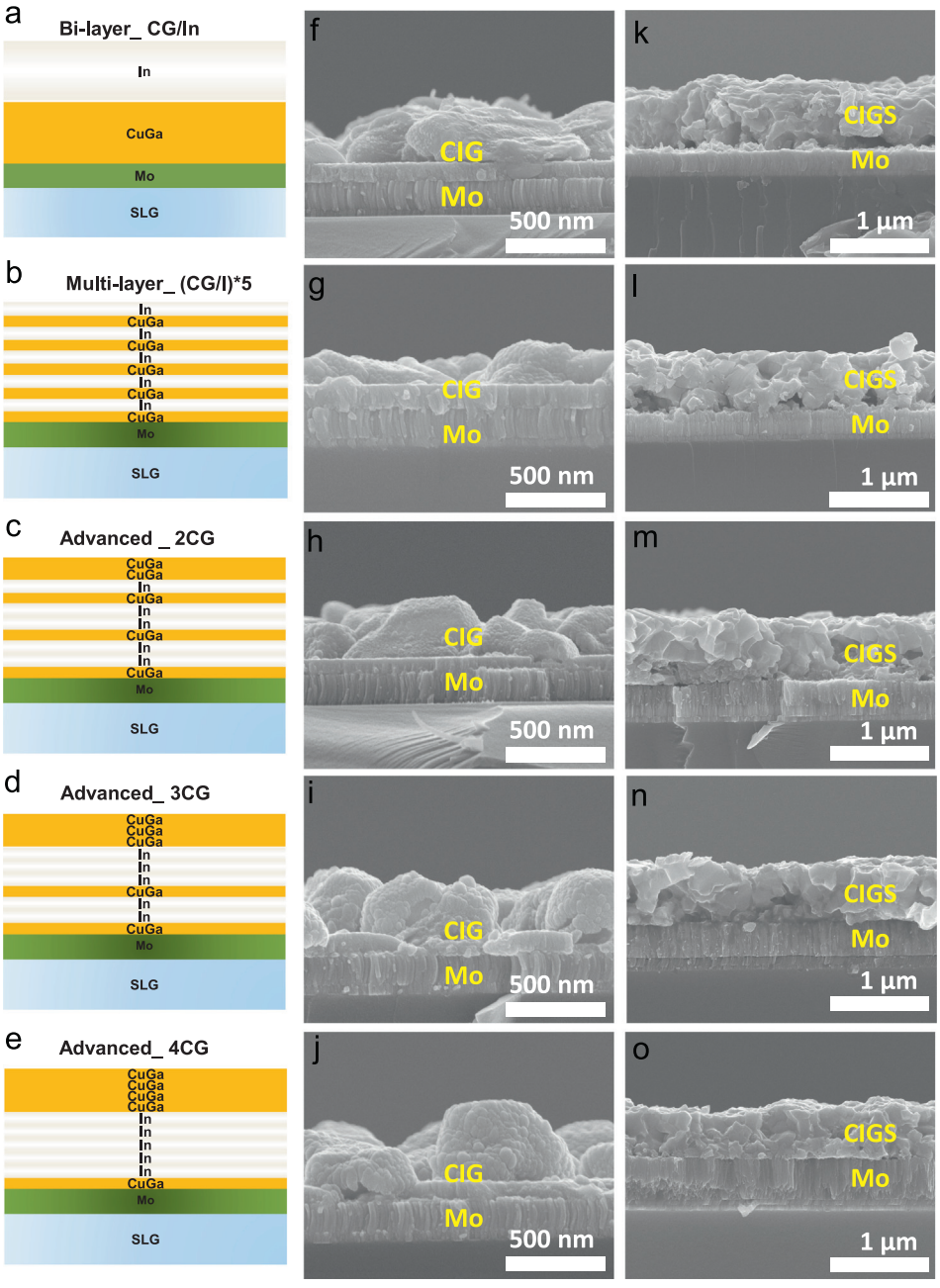

Figure 1 (a-e)Schematic images of various stacking sequences. (f-j) Cross-sectional SEM images of corresponding precursors with various roughness from In islands on flat CuGa layers. Note that the thickness for all condition is kept the same. (k-o) Cross-sectional SEM images of corresponding selenized CIGS films with different roughness and compactness extent.

because of phase separation between $CuInSe_2$ (CIS) and $CuGaSe_2$ (CGS) [11-13].

The selenization process by H_2Se gas, a conventional methodology, is usually used to provide homogeneous Ga distribution through the CIGS film. A non-toxic hydrogen-assisted solid Se vapor selenization process (HASVS) technique using non-toxic Se pellets as precursor to achieve a large-area ($40 \times 30\ cm^2$) and uniform CIGS solar panel has been demonstrated in our previous study [14]. The term, "non-toxic", was confirmed by sensing the exhausting gas with H_2Se concentration <1 ppb. In this regard, we report a symmetric study on layer stacking modification of metallic precursors to improve the qualities of the CIGS thin film, including a better crystalline structure and well control of the Ga distribution through film. Findings indicate that multi-layer precursors with modified stacking sequence can mitigate low-melting-point for In phase hillocks and increase the amount of the Ga on a surface. The detailed surface morphologies and crystalline qualities with respect to different stacking sequences and Ga distribution were investigated. In addition, a pre-annealing process at 330 °C prior to the HASVS process can stabilize the Ga distribution on surface of CIGS film, leading to a much larger bandgap (E_g) extracted by external quantum efficiency (EQE) measurements where the $Cu_{16}In_9$ intermediate phase forms first and then a Ga phase forms in the top of the film. Thus, the increased ratios of Ga to Ga and In (GGI) are observed in the space-charge region. Finally, a large-area ($40 \times 30\ cm^2$) CIGS solar panel efficiency with improved open circuit voltage (V_{OC}) and fill factor (FF) of 36% and 14% has been demonstrated, respectively, yielding the highest efficiency of $\sim$11.04% based on modified multi-layer precursors after the pre-annealing process without Se vapor followed by the HASVS process.

Experimental procedure

Process

Configuration of a CIGS solar cell typically consists of SLG/Mo/CIGS/CdS/ZnO/ ITO/Al. Soda lime Glass (SLG) with a moderate concentration of Na ions was used as substrate. A Mo back electrode on the SLG with a thickness of 0.4 μm was fabricated by two-stage sputtering processes to achieve better adhesion, higher thermal stability, and lower contact resistance, respectively [15]. The CIGS absorber layer was prepared by DC sputtering of $Cu_{0.75}Ga_{0.25}$ and In metallic targets rather than CuInGa or $CuInGaSe_2$ single target due to flexibility of composition modification, which has widely been used in mass production. Metallic precursors were sputtered on the Mo-coated SLG substrate with different stacking sequences with a fixed total thickness of $\sim$0.8 μm. The detail of following selenization follows the standard non-toxic hydrogen-assisted Se solid vapor selenization (HASVS) process at 550 °C for 20 min and the ratio of N_2 to H_2 is 15% to 85%0.[14] In addition, before the HASVS process, pre-annealing process without Se vapor at annealing temperature of $\sim$330 °C was applied. A 80 nm-thin CdS buffer layer was chemically grown on a CIGS layer via chemical bath deposition (CBD) at 70 °C. Subsequently, ZnO (70 nm)/ITO (550 nm) layers were deposited by pulsed-DC and DC sputtering systems as window/transparent conducting layers, with which the average transmittance and resistivity were $>88\%$ and $<6.0 \times 10^{-4}$ Ω-cm, respectively. Finally, an Al electrode with a thickness of 1 μm was deposited on the top by the DC sputtering system.

Characterization

Morphologies and microstructures of CIGS thin films were performed by field emission scanning electron microscopy (FESEM JSE-6500 F) equipped with electron dispersive spectrometer (EDS). X-ray photoelectron spectroscopy (XPS, Thermo Fisher Scientific Theta Probe) was used to detect the compositional changes in the CIGS film. Glance incident angle X-ray diffraction (GIXRD) with a copper target (Kα; $\lambda =$ 0.154 nm) was used to inspect phase orientations and crystalline quality at fixed incident angle of 0.5° from surface of sample. Current-voltage characteristics of solar cell were measured using Keithley 2400 source-meter illuminated by a standard AM 1.5 G (Class AAA Solar Simulator, Newport) with a power of 1000 W/m^2. The temperature was actively controlled at 25 ± 1 °C during the measurements. External quantum efficiency (EQE) was measured by a system of mercury spectrum lamp, optical emission spectrometer, and lock-in amplifier with measurements ranged from 200 nm to 1800 nm. Short circuit current was verified by the EQE spectrum calibrated by the AM1.5G standard solar simulator spectrum (ASTM G173-03). Bandgap was extracted from the EQE spectrum by using $[h\nu \times \ln(1-EQE)]^2$ versus $h\nu$ [16,17].

Results and discussion

Microstructures and composition changes with different stacking sequences of metallic precursors

Figure 1(a-e) shows the schematics of different stacking sequences of metallic precursors. Figure 1(f-j) and 1(k-o) shows the corresponding cross-sectional SEM images before and after the HASVS process, respectively. The top-view SEM images are shown in Figure S1. Note that the conventional stacking sequence, In/CuGa/Mo, was marked as "Bi-layer" while the CuGa layer is as bottom layer for the CIGS/Mo adhesion consideration (Figure 1a). Obviously, the rough surfaces of precursors are observed in the bi-layer sample as shown in Figure 1(f). The rough surfaces are most likely from formation of hillocks owing to coalescence of In islands occurred by the compressive stress due to a low melting point and high diffusion coefficient without inserting the CuGa layer as deposition time increases [18,19]. To tackle the surface roughness issue, we shorten the In deposition time by using multi-steps (five steps in this study) in order to maintain the same thickness while the CuGa layer was inserted into each step to avoid the formation of In islands. For different layer stacking modifications, each CuGa or In layer with one fifth thickness of bi-layer structure were used while the CuGa layer was used as the bottom layer. Therefore, four kinds of stacking sequences of metal precursors were investigated to increase the Ga concentrations on the surface of the CIGS film as follows, In/CuGa/In/CuGa/In/CuGa/In/CuGa/In/CuGa/Mo, denoted as "Multi-layer" (Figure 1b), CuGa/CuGa/In/CuGa/In/In/CuGa/In/In/CuGa/

Mo, denoted as "Advanced_ 2CG" (Figure 1c), CuGa/CuGa/CuGa/In/In/In/CuGa/In/In/CuGa/Mo, denoted as "Advanced_ 3CG" (Figure 1d), and CuGa/CuGa/CuGa/CuGa/In/In/In/In/CuGa/Mo, denoted as "Advanced_ 4CG" (Figure 1e), respectively. As can been seen in cross sectional SEM images (Figure 1g–j), more CuGa stacking layers can lead to much rougher morphology with highly dense In islands. In the ultimate case, namely, advanced_4CG as shown in Figure 1 (e), the equivalent effect of single and thick In layer was formed. Therefore, the obvious island structures were observed again where the morphology of samples after the HASVS process exhibits slightly correlation to this trend, as shown from Figure 1(k–o). The higher In islands can lead to rougher and larger islands confirmed by the top view SEM images (Figure 1f–j corresponding to Figure S1f–j), respectively. By plotting volume sizes of In islands taken from SEM images as the function of vertical height of In islands at different stacking sequences of metallic precursors as shown in Figure S2, it is obviously that the smaller size and higher In islands lead to flat and compact films after the HASVS process (Figure 1k–n corresponding to Figure S1k–n) so that the "flatter" and "smaller" island structures were observed in the advanced_2CG structure. This is why the CIGS phase with compact films and larger grain can be found for the stacking sequences of the advanced_2CG after the HASVS process as show in Figure S1(m) and Figure 1(m).

Figure 2(a) shows Ga concentration profiles of CIGS thin films with different stacking sequences of metallic precursors obtained by XPS measurements at an ion beam etching rate of ~0.35 nm/s after the HASVS process. The detailed Ga concentration profiles close to the surface of CIGS thin films is shown in Figure S3 (surface to 300 nm in depth). Obviously, significant Ga segregation toward the bottom of the CIGS film can be found after the HASVS process for all different stacking sequences (Figure 2a). Note that a Ga depleted region for the bi-layer case at depth between 30 and 270 nm from the surface of the CIGS thin film case was found while the Ga depleted region get much improvement after modification of stacking consequences (Figure S3). Furthermore, the Ga concentration increases at the surface of the CISG film (<30 nm) as numbers of top CuGa layers increase, namely, advanced_2CG to advanced 4CG, respectively (Figure S3). The higher Ga content in the surface will lead to higher band gap, thus larger open circuit voltage (V_{OC}) might be obtained with advanced stacking structures and will be discussed later. In addition, Figure 2(b) shows CIGS (1 1 2) orientation for different stacking sequences of metal precursors obtained by GIXRD in order to confirm the transformation of crystalline phase. In JCPDS (International Centre for Diffraction Data) database, the (1 1 2) orientation of $CuInSe_2$ is located at 2θ=26.6° and $CuGaSe_2$ is located at 2θ=27.8° as marked in dash lines in Figure 2 (b). Consequently, no $CuGaSe_2$ phase forms while Cu(In,Ga)Se_2 phase with a red shift with respect to $CuInSe_2$ was observed. The broaden peak with the red shift to larger 2θ value of the Cu(In,Ga)Se_2 phase is attributed to higher Ga contents at the surface of the CIGS film as the numbers of GaCu layers increase [20]. In addition, the higher Ga contents at the surface of the CIGS film will further result in phase separation phenomena (one at 26.7° and another at 27.2°), namely Ga-poor and Ga-rich phases. The location of Ga-poor phase slightly increases, corresponding to the trend of XPS depth profiles owing to the increased Ga content at the surface of the CIGS film as numbers of top CuGa layers increase. The phase separation phenomena eventually deteriorate device performance. As a result, the advanced_2CG configuration exhibits the less phase separation than other structures and shows a more uniform structure in depth.

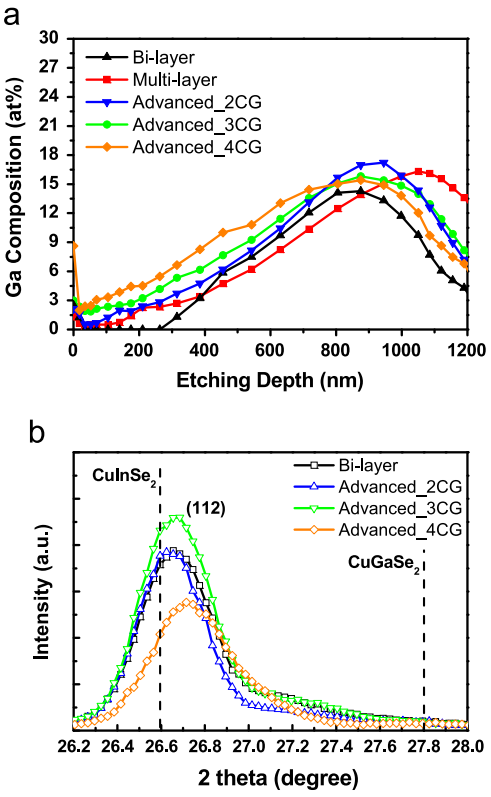

Figure 2 (a)Ga compositional depth profiles of various stacking sequences in XPS analysis. Depth is defined by etching time represented by ion gun sputtering. (b) XRD spectra of CIGS (1 1 2) crystalline orientation for all kinds of stacking sequences.

Effects and efficiency measurements of CIGS solar cell with different stacking sequences of metallic precursors and improved efficiency after pre-annealing process without Se vapor at low temperature

To shed light on energy conversion performance, the CIGS thin films with different stacking sequences of metal precursors were preceded by a standard device fabrication process, namely Al/ITO/i-ZnO/CdS/CIGS/Mo/SLG (see experimental part for more detailed information). The corresponding *J*-*V* curves of bi-, multi-, and advanced_2CG after the HASVS process were measured under AM1.5 G solar simulator as shown in Figure 3(a). The corresponding conversion efficiency (η), filling factor (FF), short circuit current (J_{SC}), and open circuit voltage (V_{OC}) are listed in Table 1, respectively. Obviously, the V_{OC} can be clearly enhanced from 0.41 V for bi-layer to 0.53 V after the multi-layer stacking modification due to formation of high Ga contents on the surface of the CIGS film confirmed by elemental profiles. Interestingly, as the

number of the CuGa layers increases, the energy conversion performance for the *J-V* curve reveals improved V_{OC} from 0.53 V for the advanced_2CG to 0.56 V for the advanced_4CG as shown in Figure 3(b) (Figure S4). Moreover, enhancement of FF are achieved by improving the smoothness and compactness of the surface after the HASVS process while both J_{SC} from 30.76 mA/cm^2 for the advanced_2CG to 27.27 mA/cm^2 for the advanced_4CG with η from 10.10% for the advanced_2CG to 9.60% for the advanced_4CG are degraded as numbers of CuGa layers increase. The degradation of the performance for the advanced_4CG is supposed to be the phase separation. Consequently, a maximum performance of efficiency reaching to ~10.1% can be achieved for the advanced_2CG case.

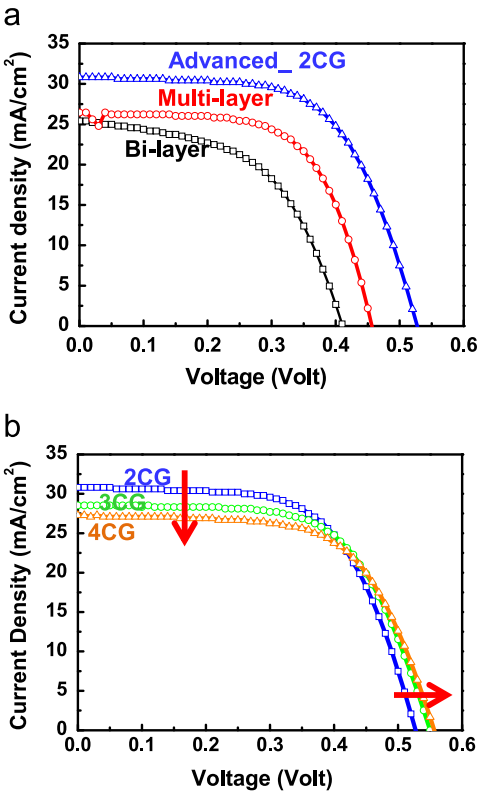

Figure 3 (a)Representative *J-V* characteristics of CIGS devices with Bi-layer/Multi-layer/Advanced_2CG stacking sequences. (b) *J-V* characteristics comparison of CIGS devices with further stacking Ga on top (Advanced_2CG/Advanced_3CG/Advanced_4CG).

As can be proved by XPS measurements, Ga can be segregated in depth of 30 nm beneath the surface of the CIGS film after using stacking sequences of metal precursors. It is well known that pure CIGS phase forms only at a high temperature >450 °C and a long dwell time more than 20 min while the interdiffusion of In and Ga occurs. In addition, the reaction kinetics reveals that the activation energy of CIS phase (~124 kJ/mol) is lower than that of CIGS phase (~144 kJ/mol), indicating that the CIS phase has lower surface free energy than the CGS phase [21]. Therefore, the CIS phase is preferentially formed on the surface rather than CIGS phase and Ga atoms are enforced to diffuse toward to the bottom of the CIGS film through grain boundary or vacancy defects during the selenization process [22,23]. To tackle the problem, the gas phase selenization process using H_2Se is widely used to homogenize the Ga distribution in depth while safety concerns owing to toxic issue and facility cost have to be taken into account. Other previous studies reported that Se comes from the precursors at low temperature and form a Se amorphous phase to retard the Ga diffusion toward the bottom of the CIGS films [24]. Here, a process, called the pre-annealing process at 330 °C for 40 min on the pure CIG precursor, was applied to prevent Se segregation during the HASVS process (Figure S5). The pre-annealing process prior to the HASVS process is also considered to further enhance Ga distribution along the surface of the CIGS film. As a result, the efficiency can be further improved to ~11.4% for the Advanced_2CG case after the pre-annealing process followed by the HASVS process as listed in Table 1. The reason of the pre-annealing process at 330 °C on pure CIG precursor is due to the complete formation of $Cu_{16}In_9$ phase (ref. code 01-071-7753) with remaining Ga phase (ref. code 01-089-2735) at the specific composition ratio near stoichiometry confirmed by the GIXRD spectra as shown Figure 4(a) [25]. The corresponding elemental profiling of Ga is kept in the top of thin film surface and thus there is no vacancy defects formed as shown in Figure 4(b). For comparison, the same sample annealed at 330 °C without the pre-annealing process (i.e. with Se vapor participation) shows formation of low activation energy CIS phase (ref. code 00-035-1102) and Cu_xSe secondary phase (ref. code 00-049-1457), respectively, for which the Ga atoms are "pushed" toward the bottom of the CIGS film. XPS analysis verifies this

Table 1 List of CIGS solar cell performance (conversion efficiency/fill factor/short circuit current/open circuit voltage) with different stacking sequences of metal precursors and different selenizaton profiles.

Stacking structure	Selenization profile	η (%)	FF (%)	J_{sc} (mA/cm^2)	V_{oc} (V)
Mo-CuGa/In (Bi-layer)	HASVS	5.53	52.8	25.50	0.41
Mo-CuGa/In/CuGa/In/CuGa/In/CuGa/In/CuGa/In (Multi-layer)	HASVS	7.61	62.5	26.45	0.46
Mo-CuGa/In/In/CuGa/In/In/CuGa/In/CuGa/CuGa (Advanced_2CG)	HASVS	10.10	61.7	30.76	0.53
Mo-CuGa/In/In/CuGa/In/In/In/CuGa/CuGa/CuGa (Advanced_3CG p)	HASVS	9.80	62.9	28.55	0.55
Mo-CuGa/In/In/In/In/In/CuGa/CuGa/CuGa/CuGa (Advanced_4CG)	HASVS	9.60	62.5	27.27	0.56
Mo-CuGa/In/In/CuGa/In/In/CuGa/In/CuGa/CuGa (Advanced_2CG)	Pre-annealing process +HASVS	11.04	60.4	32.70	0.56

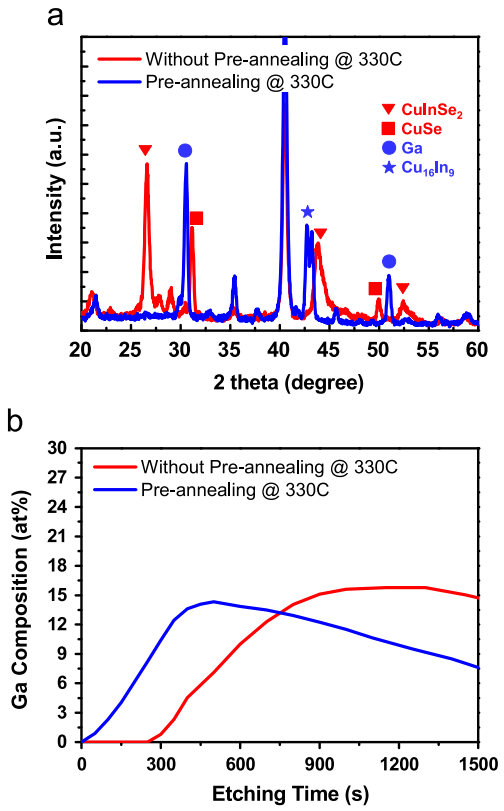

Figure 4 (a)XRD spectrum of the Advacne_2CG samples with and without the pre-annealing processes at 33 °C. (b) Corresponding Ga compositional depth profiles for two kinds of CIGS films.

observation as shown in Figure 4(b). This is why no Ga signal can be found in GIXRD results. Note that the results of the Ga profile [26] are the results of Ga accumulation near the bottom of the film and In-Ga interdiffusion. As a result, the same with the pre-annealing process remains more Ga on the top of thin film surface than the sample without the pre-annealing process, resulting in high Ga contents and high GGI ratios (Ga /Ga+In) confirmed by elemental depth profiles from XPS measurements as shown in Figure S6.

Fabrication of panel scale 30×40 cm^2 toward high efficiency Cu(In,Ga)Se$_2$ solar cell

Furthermore, we repeat the standard device fabrication processes to fabricate a panel size CIGS solar with 30×40 cm^2 in width and length without and with the pre-annealing processes followed by the HASVS process, respectively. The corresponding images of the advanced_2CG sample for two kinds of conditions are shown in Figure 5 (a) and (b). Clearly, a lot of dark spots were observed in the sample without the pre-annealing process while the uniform surface of the CIGS film can be achieved with the pre-annealing process. It is because solid Se vapor might cause severe Se condensation at a substrate temperature <330 °C because of incomplete reaction during the following HASVS process. Insets in Figure 5(a) and (b) shows the corresponding SEM images for two cases. As can be seen in top view SEM images, the larger average grain size of $\sim$1.3 μm was observed after the pre-annealing process. However, the grain size of $\sim$1 μm was found without the pre-annealing process. The improvement of the grain size might be the stabilization of precursor with stoichiometric distribution, thus the uniform grain size in lateral or in depth (as shown in cross sectional view SEM) are formed. The average efficiency of $\sim$8.25% for the advanced_2CG samples after the HASVS process without pre-annealing process were measured by measuring more than 25 devices with actively measured area of 0.48 cm^2 while the average conversion efficiency of $\sim$9.29% and the champion cell as high as the efficiency of $\sim$11.0% (12.2% with active area) can be achieved with the pre-annealing process followed by the HASVS process as shown in Figure 5(c). The corresponding parameters are also listed in Table 1. Furthermore, photo responses in EQE measurements were measured, indicating that the enhanced efficiency is due to the improved quantum efficiency because of higher absorption at visible wavelength region (Figure S7). The larger band gap is attributed to the higher Ga concentrates in the CIGS film for the advanced_2CG sample after the pre-annealing process compared with the same sample without the pre-annealing process prior to the HASVS process. This is why the significantly enlarged V_{OC} of $\sim$6% is resulted from the larger Ga concentrations at the surface of CIGS film and increased J_{SC} of $\sim$6% was also found due to larger grain size and compact microstructure, yielding the enhanced cell efficiency of CIGS solar cell. To shed light on enlarged band gap due to the higher concentration of Ga atoms in the CIGS film, the energy band gaps of the CIGS thin films for the advanced_2CG with two kinds of annealing processes were extracted from EQE measurements as shown in Figure 5(d). Obviously, the average band gap of the sample after the pre-annealing process film is 1.08 eV, which is larger than that of the same sample without the pre-annealing process (1.02 eV). For the process integration consideration, the pre-annealing process can be also applied at extremely low cost non-vacuum process such as particle-based CIGS [27] and CZTS [28,29]. In addition, pre-annealing process can stabilize the precursor and get free of detrimental oxygen and carbon to CIGS or CZTS thin film solar cells[24]. Our results provide a facile approach for quality improvement of CIGS and stimulate a low cost, high output, and non-toxic procedure in large scale CIGS PV industries.

Conclusions

We have demonstrated an optimized precursor stacking sequences to achieve a large-area (40×30 cm^2) CIGS solar panel. The conversion efficiency can be enhanced as high as 11.0% (12.2% for active area). An increased Ga segregation on the top of the thin film was achieved by the stacking of multi-layer with two CuGa layers on top, namely advanced_2CG and the smooth and compact microstructure was obtained as well. Furthermore, a pre-annealing process at low temperature of 330 °C was applied which can retain high Ga concentration on the surface of the thin films by forming $Cu_{16}In_9$ phase and pure Ga phase while the sample without the pre-annealing, the CIS phase is formed first and

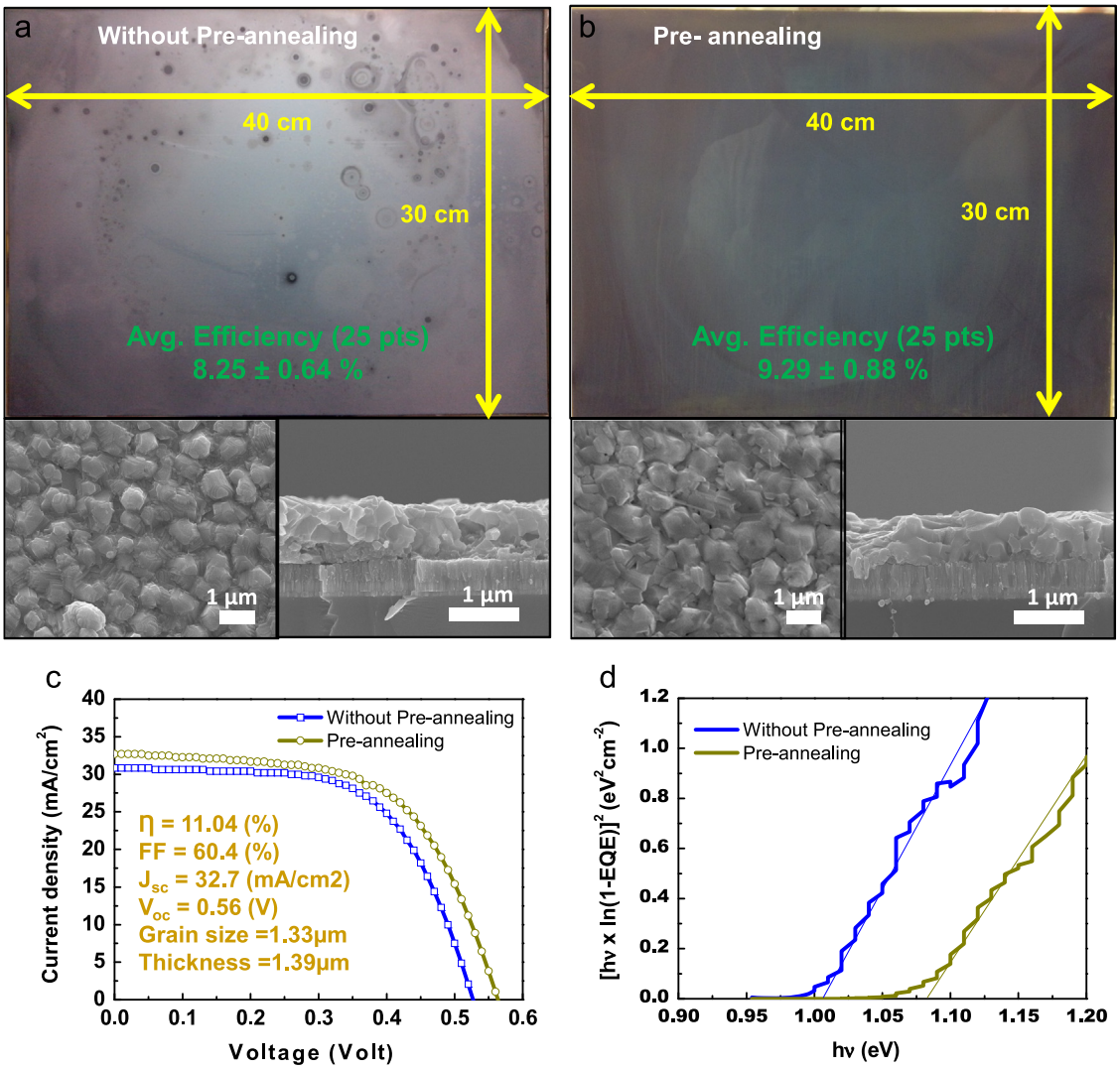

Figure 5 (a) and (b) Comparison between with and without the pre-annealing process for the CIGS solar panel for the Advance_2CG. Insets show the corresponding top-view and cross-sectional SEM images. (c) Comparison of the champion cell performance with and without the pre-annealing process. (d) Band gaps (E_g) for the Advance_2CG sample with and without the pre-annealing process extracted from EQE measurements.

then repels Ga toward to the bottom of the CIGS thin film. As a result, high GGI ratio was observed and high energy band gap can be achieved, yielding an improved V_{OC} to 0.56 V and the highest efficiency of ~11% for the advanced_2CG sequence with the pre-annealing process followed by the HASVS process.

Acknowledgments

The authors gratefully thanks to Ministry of Science and Technology through Grant nos. 101-2218-E-007-009-MY3, 102-2633-M-007-002, 101-2622-E-492-001-CC2, and National Tsing Hua University through Grant no., 102N2022E1. Y. L. Chueh greatly appreciates the use of facility at CNMM the National Tsing Hua University through Grant no., 102N2744E1.

Appendix A. Supporting information

Supplementary data associated with this article can be found in the online version at http://dx.doi.org/10.1016/j.nanoen.2014.07.018.

References

[1] K. Kushika, Sol. Energy Mater. Sol. Cells 93 (2009) 1037–1041.
[2] S. Niki, M. Contreras, I. Repins, M. Powalla, K. Kushika, S. Ishizuka, K. Matsubara, Prog. Photovolt. 18 (2010) 453–466.
[3] ZSW produces world record solar cell – Thin-film photovoltaics achieves 20.8% efficiency and overtakes multicrystalline silicon technology, (2013) ⟨http://www.zsw-bw.de/en/support/ press-releases/press-detail/zsw-stellt-weltrekord-solarzelle-her.html⟩.
[4] M.A. Green, K. Emery, Y. Hishikawa, W. Warta, E.D. Dunlop, Prog. Photovolt. 21 (2013) 827–837.

[5] N.G. Dhere, K.W. Lynn, Sol. Energy Mater. Sol. Cells 41–42 (1996) 271–279.
[6] S.D. Kim, H.J. Kim, K.H. Yoon, J.S. Song, Sol. Energy Mater. Sol. Cells 62 (2000) 357–368.
[7] W. Li, Y. Sun, W. Liu, L. Zhou, Solar Energy 80 (2006) 191–195.
[8] O. Volobujeva, M. Altosaar, J. Raudoja, E. Mellikov, M. Grossberg, L. Kaupmees, P. Barvinschi, Sol. Energy Mater. Sol. Cells 93 (2009) 11–14.
[9] C.D. R. Ludwig, T. Gruhn, C. Felser, T. Schilling, J. Windeln, P. Kratzer, Phys. Rev. Lett. 105 (2011) 025702.
[10] D.J. Schroeder, G.D. Berry, A.A. Rockett, Appl. Phys. Lett. 69 (1996) 4068–4070.
[11] S.H. Wei, S.B. Zhang, A. Zunger, Appl. Phys. Lett. 72 (1998) 3199–3201.
[12] T. Dullweber, O. Lundberg, J. Malmstrom, M. Bodegard, L. Stolt, U. Rau, H.W. Schock, J.H. Werner, Thin Solid Films 387 (2001) 11–13.
[13] O. Lundberg, J. Lu, A. Rockett, M. Edoff, L. Stolt, J. Phys. Chem. Solids 64 (2003) 1499–1504.
[14] T.T. Wu, F. Hu, J.H. Huang, C.H. Chang, C.C. Lai, Y.T. Yen, H.Y. Huang, H.F. Hong, Z.M. Wang, C.H. Shen, J.M. Shieh, Y.L. Chueh, ACS Appl. Mater. Interfaces 6 (2014) 4842–4849.
[15] Yoon, J. H.; Cho, S.; Seong, T. Y.; Jeong, J. H. Optical Diagnosis of the Microstructure of Mo Back Contact for CIS Solar Cell 216th ECS Meeting 2009.
[16] M. Altosaar, J. Raudoja, K. Timmo, M. Danilson, M. Grossberg, J. Krustok, E. Mellikov, Phys. Status Solidi A 205 (2008) 167–170.
[17] G. Zoppi, I. Forbes, R.W. Miles, P.J. Dale, J.J. Scragg, L.M. Peter, Prog. Photovolt. 17 (2009) 315–319.
[18] C.H. Chung, S.D. Kim, H.J. Kim, F.O. Adurodija, K.H. Yoon, J. Song, Solid State Commun. 126 (2003) 185–190.
[19] H.L. Wei, X.X. Zhang, H.C. Huang, Chin. Phys. Lett. 23 (2006) 1880–1883.
[20] D.J. Schroeder, J.L. Hernandez, G.D. Berry, A.A. Rockett, J. Appl. Phys. 83 (1998) 1519–1526.
[21] W.K. Kim (Ph.D. Thesis), University of Florida, 2006.
[22] R. Caballero, C. Guillen, M.T. Gutierrez, C.A. Kaufmann, Prog. Photovolt. 14 (2006) 145–153.
[23] M. Marudachalam, R.W. Birkmire, H. Hichri, J.M. Schultz, A. Swartzlander, M.M. Al-Jassim, J. Appl. Phys. 82 (1997) 2896–2905.
[24] D.G. Moon, J.H. Yun, J. Gwak, S.K. Ahn, A. Cho, K. Shin, K. Yoon, S.J. Ahn, Energy Environ. Sci. 5 (2012) 9914–9921.
[25] M. Purwins, R. Enderle, M. Schmid, P. Berwian, G. Muller, F. Hergert, S. Jost, R. Hock, Thin Solid Films 515 (2007) 5895–5898.
[26] E. Rudigier, J. Djordjevic, C. Klopmann, B. Barcones, A. Perez-Rodriguez, R. Scheer, J. Phys. Chem. Solids 66 (2005) 1954–1960.
[27] G. Chen, W Liu, G. Jiang, C. Zhu, J. Alloys Compd. 531 (2012) 91–95.
[28] Y. Lin, S. Ikeda, W. Septina, Y. Kawasaki, T. Harada, M. Matsumura, Sol. Energy Mater. Sol. Cells 120 (2014) 218–225.
[29] S. Ahmad, K.B. Reuter, O. Gunawan, L. Guo, L.T. Romankiw, H. Deligianni, Adv. Energy Mater. 2 (2012) 253–259.

Tsung-Ta Wu received his M.S. degree from Department of Materials Science and Engineering, National Tsing Hua University, Taiwan in 2006. Now he is a Ph.D. candidate at department of materials science and engineering, National Tsing Hua University. He also works in National Nano Device Laboratories in Taiwan, his research interests include: CIGS solar cell research, semiconductor process integration and circuit layout design.

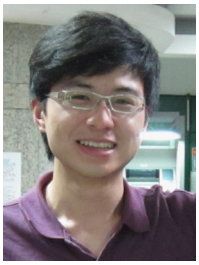

Jyun-Hong Huang was born in Kaohsiung, Taiwan, in 1989. He received his B.S. degree in electronic engineering from Chang Gung University (CGU), Taoyuan, Taiwan and M.S. in Imaging and Biomedical Photonics from National Chiao Tung University (NCTU), Hsinchu, Taiwan in 2011 and 2013, respectively, and now he is a Ph.D. student in electronics engineering of National Chiao Tung University.

Fan Hu received his M.S. degree from Department of Materials Science and Engineering, National Tsing Hua University, Taiwan in 2013. Now he is an engineer and works in TSMC Solar, Taiwan.

Chia-Ho Chang received his M.S. degree from Department of Optoelectronic Engineering, National Chung Hsing University, Taiwan 2010. Now he is an engineer and works in National Nano Device Laboratories, Taiwan.

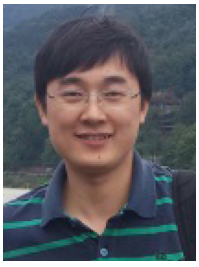

Wen-Long Liu is a Postdoctoral researcher at the National Tsing Hua University in Prof. Yu-Lun Chueh's group. He received his Ph.D. at the School of Chemical Engineering from Sichuan University, Chengdu, China, in 2012. During his Ph.D. work, he focused on the synthesis, self-assembly of nanomaterials, for development of the functional materials in the application of thin-film solar cells. His postdoc work is focuses on the development of thin-film solar cells using an earth-abundant material, kesterite, as absorber, and, particularly, by non-vacuum processing. His expertise is in the field of nanomaterials related chemistry and materials devices.

Tsang-Hsiu Wang Wang received his Ph.D degree from Department of Chemistry, University of Alabama, USA in 2010. From 2010 to 2012, he was as a postdoctoral research fellow in University of Taipei, Taiwan. Besides, he also worked at Institute of Atomic and Molecular Science (IAMS), Taiwan as a postdoctoral research scholar from 2012 to 2013. Then, he joined Dr. Chueh's group as a postdoctoral research fellow in 11/2013. His research interests include properties of metal-oxide nanoparticles and nanoclusters and design of photosensitizes.

Chang-Hong Shen received his Ph.D. in Physics at National Tsing-Hua University in 2006. From 2007, he joined MOSEL VITELIC INC in Taiwan. From 2009, he joined National Nano Device Laboratories as associate researcher. Currently he is a Research fellow and Division Director of advanced device division in NDL. His academic interests include photovoltaic devices, flexible electronics, and low-temperature laser/plasma

processing. His current research focuses on developing low-cost, third-generation Si and CIGS thin-film solar cells, and low-temperature 3D nanoelectronics. Details can be found at: http://www.ndl.narl.org.tw/web/eng/research/ENERGY_Manpower.php.

Jia-Min Shieh received his Ph.D. in Electro-Optics at National Chiao-Tung University, Taiwan in 1997. From 1998, he joined National Nano Device Laboratories (NDL), Taiwan and became a researcher from 2003. He leads the photovoltaic/photonic device division and Emerging Device Division in NDL from 2008 to 2013. Currently he is Deputy Director General in NDL. His academic interests include photovoltaic/photonic devices, flexible electronics, and low-temperature laser/plasma processing. His current research focuses on developing low-cost, third-generation Si and CIGS thin-film solar cells, Si quantum-dot photovoltaic/photonic/electronic devices, and low-temperature 3D nanoelectronics. Details can be found at: http://www.ndl.narl.org.tw/web/research/JMShieh.php.

Yu-Lun Chueh received his Ph.D degree from Department of Materials Science and Engineering, National Tsing Hua University, Taiwan in 2006 and worked as postdoctor in electrical engineering and computer science, UC Berkeley from 2007 to 2009. He joined department of materials science and engineering, National Tsing Hua university in 2009. His research directions include (1) syntheses of energy materials and its applications in solar energy harvesting, (2) performance enhancement of resistive change memory, and (3) synthesis of graphene and its application in nanodevices, and development of desalination from sea water. Details can be found at: http://nanoscienceandnanodevicelab.weebly.com/index.html.